THE JOURNAL OF PHYSICAL CHEMISTRY B

 VOLUME 104, NUMBER 41, OCTOBER 19, 2000

LETTERS

Evidence for Spinodal Phase Separation in Two-Dimensional Nanocrystal Self-Assembly

Guanglu Ge* and Louis Brus

Department of Chemistry, Columbia University, New York, New York 10027

Received: June 27, 2000; In Final Form: August 22, 2000

The drying of thin nanocrystal solution films creates a varied range of structured aggregate spatial patterns as a function of surface coverage. These images can be understood as predicted kinetic stages in the fluid-fluid spinodal phase separation of a 2D van der Waals particle system. It is suggested that phase separation occurs due to increased van der Waals nanocrystal−nanocrystal interaction in the presence of air, as compared with the shielded interaction in organic solvents.

Metallic and semiconducting nanocrystals with organic surface ligands can serve as "superatom" building blocks for complex thin film materials. A key issue is understanding natural self-assembly from solution. Under optimal conditions crystalline 2D and 3D nanocrystal solids can be grown.[1−4] For example, at the air:water interface initially dilute 3 nm Au nanocrystals self-assemble into a 2D crystalline phase with increasing lateral pressure.[5] Korgel and Fitzmaurice have suggested that Au nanocrystal aggregates on graphitic TEM grid surface can be treated as wetting films, and have estimated the surface tensions.[6] The fundamental questions of nanocrystal-solvent phase diagrams, and the interaction potential between two solvated nanocrystals, however remain poorly understood, and additionally in 2D should dependent upon local environment. In this work we study 2D growth kinetics, and show that the spatial patterns are kinetic stages in fluid-fluid spinodal nucleation and subsequent coarsening. We suggest that the drying process acts as a quench of the reduced temperature, below the critical temperature into the unstable spinodal region, because of an increased van der Waals interaction in a 2D layer. On this surface the 2D nanocrystal phase diagram is closer to the classical three phase (solid−liquid-gas) diagram of van der Waals particles, rather than the two phase diagrams of hard sphere or adhesive particles.[7−9]

As previously recognized, and in contrast to polymer, silica, and biological virus particles, metallic and semiconducting nanoparticles with high dielectric constants should show significant long-range van der Waals (vdW) interaction. A simple model for the interaction energy could combine a Hamaker-Lifshitz (HL) continuum vdW attraction and a polymer brush interaction.[2−4] The long-range attraction is sufficient to induce reversible nanoparticle aggregation.[10] Energy in HL theory is expressed as the product of a geometric factor and a material-dependent factor, called the Hamaker constant. The frequency dependent dielectric functions of the interacting bodies and the surrounding medium appear in the Hamaker constant. Generally, particles experience weaker attraction when the dielectric properties of the medium in all directions are similar to those of the particles.

We study nanocrystal aggregation patterns and kinetics on smooth graphite (HOPG) using an AFM, both under organic liquid and after drying of thin wet films. Size-selected CdSe nanocrystals with standard deviation less than 5% are used. Figure 1 shows images of 4 nm CdSe nanocrystals on HOPG in chloroform solvent. At coverages of 5−50%, the nanocrystals move in successive scans. Aggregates of a few nanocrystals form and then dissolve; most nanocrystals are monomers. The nanocrystals seem to form a single lattice gas fluid phase on the smooth HOPG surface. We calculated the Hamaker constant CdSe/chloroform/CdSe for two nanocrystals interacting in

* Corresponding author. E-mail address: gg129@columbia.edu.

10.1021/jp002280a CCC: $19.00
Published on Web 09/22/2000

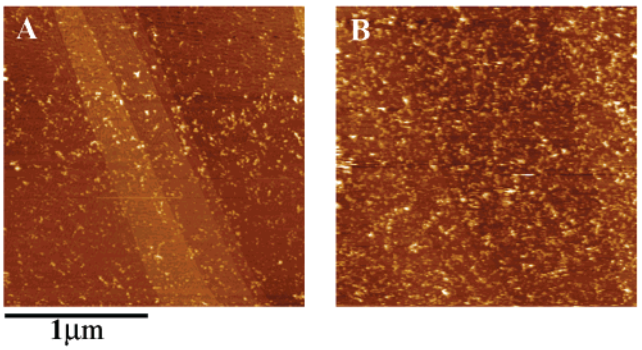

Figure 1. Liquid tapping mode AFM height images of 4 nm CdSe nanocrystals at the HOPG/chloroform interface. The nanocrystals are described in ref 1. The data are obtained with a modified liquid cell attachment on a Nanoscope III Multimode AFM. In (A) the coverage is near 5%, while in B near 50%.

chloroform solvent, and estimated the attractive vdW energy ϵ to be about $0.4kT$ at 23 °C. This single fluid phase appears consistent with a simple equilibrium 2D thermodynamic model of Israelachvili, which predicts that nanocrystals do not extensively aggregate at this weak bond strength for modest coverages.[11]

However, if the 2D system of nanocrystals is allowed to dry, very different results are observed depending upon coverage. At less than 20% coverage on a flat HOPG terrace (Figure 2b), there are many round, nearly one monolayer thick droplets, each composed of several hundred nanocrystals. Most of these droplets have a small second layer in the center, about 10% of the first layer in size for hexane solvent. The relative second layer size depends slightly yet reproducibly upon solvent, for example in chloroform it is about 1%. These results suggest, as has also been argued by Korgel and Fitzmaurice[6] for Au particles on TEM grids, that droplet shape and solid contact angle represent thermodynamic equilibrium of a "liquid" nanocrystal phase, on the HOPG surface in a thin solvent layer. The liquid nanocrystal phase strongly wets graphite. At higher AFM resolution (Figure 2c) the nanocrystals after drying show local hexagonal close-packing. In Figure 2e incipient droplet coalescence can be seen. In Figure 2d larger coalesced drops occur; in Figure 2f droplets appear to have coalesced into ribbons. These images suggest that wet droplets are mobile, before growth and coarsening is stopped by complete solvent evaporation. Patterns are highly reproducible from region to region on any single sample, but differ (as shown in Figure 2d−f) from sample to sample. If the process is stopped at very early times, smaller aggregates with very strong spatial correlation are observed (Figure 2a). Tanaka has argued that such regular spatial images of early nuclei imply that nucleation occurs by spinodal decomposition, rather than by classical random nucleation.[12]

Very regular bicontinuous patterns, whose length scale increases with time, are observed when the particle coverage is higher, around 20−30% in Figure 3a,b. These images are similar to spinodal decomposition patterns observed when a high temperature, single fluid phase polymer blend is quenched below its critical temperature and begins to phase separate. In Figure 3c a foamlike image is observed in this same coverage range.

Figure 4 is the universal van der Waals 2D phase diagram of particles interacting via Lennard-Jones type potentials.[7] In the gas−liquid coexistence region, spinodal lines separate regions of classical nucleation and barrierless spinodal nucleation.[13] The critical temperature is $T_c = 0.55$ in reduced kT/ϵ units at 32.5% coverage. In 2D computer simulations, particle systems quenched

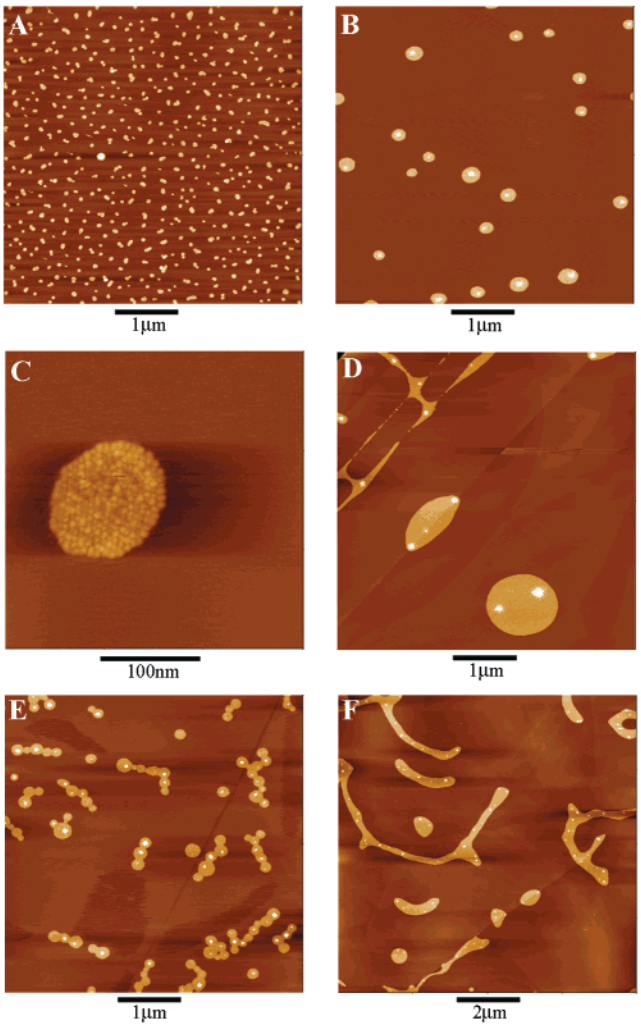

Figure 2. Air tapping mode height images of aggregates form by drying of dilute nanocrystal solutions: (A) spin coated at 150 rpm; (B, C) dried under hexane vapor in air; (D−F) dried in air. In (E) the solvent is 90% hexane/10% octane; all others are hexane. Straight lines are HOPG step edges. The first nanocrystal layer is yellow, and the second layer is white.

vertically from high to low temperature directly through T_c shows spinodal bincontinuous spatial patterns, of increasing size as gas−liquid separation proceeds in time.[14−17] An off-symmetric computer quench into the spinodal region at lower coverage shows a initially spinodal pattern that quickly evolves into liquid droplets with time. Our nanocrystal aggregation/drying process effectively behaves as a temperature quench below T_c at fixed coverage. Yet if the solvent does not evaporate (Figure 1), then we observe a single fluid phase at these same coverages; the system must be above T_c in the presence of a thick solvent layer. On rougher substrates, such as quartz and silanized quartz, only irregular small aggregates and single nanocrystals are observed after drying. Thus, assembly occurs while the nanocrystals move on the surface and not in the solution. Surface mobility is higher on HOPG.

We calculate that the Hamaker constant in a vacuum [CdSe/vacuum/CdSe] is 15.6×10^{-20} J, about four times larger than in chloroform. The calculated Hamaker constant in hexane is 30% larger than in chloroform, and the observed image patterns are similar. In the ultraviolet region where the fluctuating dielectric polarizations of two CdSe particles strongly interact, these organic solvents effectively screen the interaction. The force between two particles can be calculated using the obtained

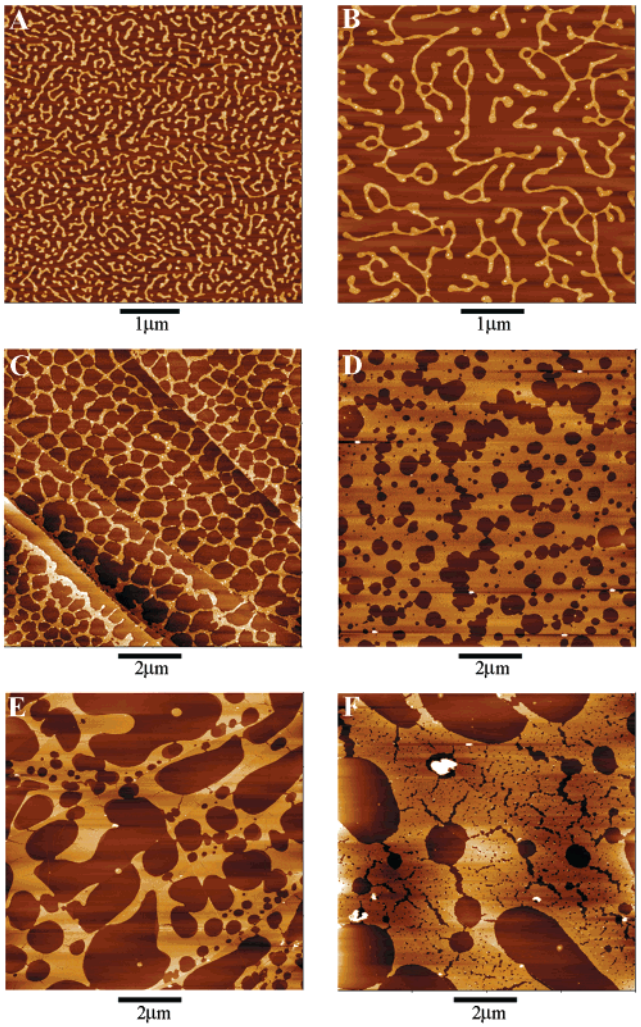

Figure 3. Air tapping mode height images at higher coverages: (A−C) chloroform solutions: (D, E) hexane solutions; (F) 10% methanol/90% chloroform solution.

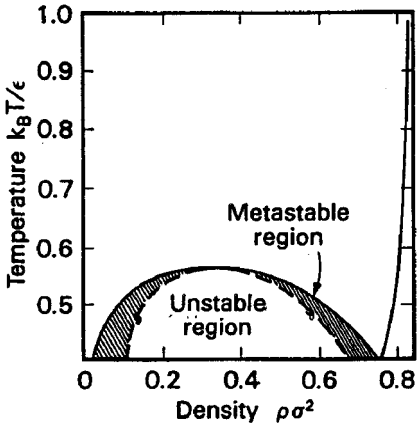

Figure 4. Universal 2D phase diagram for particles interacting via a 12-6 Lennard-Jones potential from ref 14, plotted in unitless, reduced temperature and coverage variables.

Hamaker constant and the geometric factor. Transformed into reduced temperature, this change of environment corresponds roughly to kT/ϵ of 2 (solution) and 0.5 (vacuum or air) in Figure 4. The solutions should wet graphite at all thicknesses as the film thins. The effective vdW attraction should increase as the air:solvent interface approaches the solvent:graphite interface. Near 4 nm thickness in the 2D nanoparticle/solvent film, the effective interaction ϵ must be substantially increased, which seems to bring the system from above to below the critical temperature. This new type of reduced temperature (kT/ϵ) quench with spatial dimensionally is only possible for strongly interacting inorganic particles in shielding solvents. Solvents are initially selected for high nanocrystal solubility. High 3D solubility partially reflects strong vdW solvent shielding. In thin films this shielding is reduced, and these systems then nucleate.

In 2D at low coverage, the wet nanocrystal droplets are mobile, and appear to coalesce and coarsen in a liquidlike fashion as predicted in computer simulations.[14−17] At near 60% coverage in Figure 3d the nanocrystal layer has included round holes. Such high coverage spatial patterns are also observed in 2D computer quenches, which show round bubbles of particle gas inside a particle liquid layer. Coarsening occurs as liquid droplets and/or bubbles fuse; suggestive images appear in the Figures 2c, 3d, and 3e. The effective nanocrystal fluid viscosity must be higher in the last stages of drying because we sometimes observe quenched ribbons of bubbles/droplets that have not yet coalesced into a single large bubble/droplet. Note the inverse symmetry between Figures 2e and 3d. Also note that we have never observed an isolated nanocrystal on a dry HOPG surface. We suspect that individual nanocrystals in the gaseous regions are swept by the AFM tip during scanning.

Very large nanocrystal monolayers sometimes crack upon drying as in Figure 3f. As a large wet nanocrystal layer dries the interparticle distance shrinks. The wet nanocrystal 2D liquid phase, which is less dense than the wet crystalline 2D phase in Figure 4, includes solvent between nanocrystals. As an aggregate layer completely dries, interstitial solvent evaporates, the vdW interaction increases, and interparticle distance shrinks. Shrinkage while drying has been previously monitored in real time for 3D Ag nanocrystal crystalline solids.[18] Even after drying the particle−particle separation is measured to be 2−3 nm, larger than previously reported for 3D CdSe nanocrystal solids.[1]

Acknowledgment. We enjoyed stimulating discussions with D. A. Weitz, W. B. Russel, B. J. Berne, and members of the Columbia MRSEC group. This work is supported under MRSEC DMR-98-09687. We thank the W. M. Keck Foundation for an equipment grant.

References and Notes

(1) Murray, C. B.; Kagan, C. R.; Bawendi, M. G. *Science* **1995**, *270*, 1335.
(2) Collier, C. P.; Vossmeyer, T.; Heath, J. R. *Annu. Rev. Phys. Chem.* **1998**, *49*, 371.
(3) Whetten, R. W.; et al. *Acc. Chem. Res.* **1999**, *32*, 397.
(4) Korgel, B. A.; Fitzmaurice, D. *Phys. Rev. B* **1999**, *59*, 14191.
(5) Heath, J. R.; Knobler, C. M.; Leff, D. *J. Phys. Chem.* **1997**, *101*, 189.
(6) Korgel, B. A.; Fitzmaurice, D. *Phys. Rev. Lett.* **1998**, *80*, 3531.
(7) Barker, J. A.; Henderson, D.; Abraham, F. F. *Physica* **1981**, *106A*, 226−238.
(8) Ilett, S. M.; et al. *Phys. Rev. E51* **1995**, 1344−1252.
(9) Rosenbaum, D.; Zamora, P. C.; Zukoski, C. F. *Phys. Rev. Lett.* **1996**, *76*, 150−153.
(10) Ohara, P. C.; et al. *Phys. Rev. Lett.* **1995**, *75*, 3466.
(11) Israelachivili, J. N.; *Intermolecular and Surface Forces*, 2nd ed.; Academic: New York, 1992; Chapter 16.
(12) Tanaka, H. et al. *Phys. Rev. Lett.* **1990**, *65*, 3136−3139.
(13) Debenedetti, P. G.; et al. *J. Phys. Chem. B* **1999**, *103*, 7390.
(14) Koch, S. W.; Desai, R. C.; Abraham, F. F. *Phys. Rev.* **1983**, *A27*, 2152.
(15) Wagner, A. J.; Yeomans, J. M. *Phys. Rev. Lett.* **1998**, *80*, 1429−1432.
(16) Tanaka, H.; Araki, T. *Phys. Rev. Lett.* **1998**, *81*, 389−392.
(17) Sofonea, V.; Mecke, K. R. *Eur. Phys. J.* **1999**, *B8*, 99−112.
(18) Connolly, S.; et al. *J. Am. Chem. Soc.* **1998**, *120*, 2969.